Journal of the Korean Nuclear Society
Volume 32, Number 2, pp.128~141, April 2000

Critical Heat Flux in Uniformly Heated Vertical Annulus Under a Wide Range of Pressures 0.57 to 15.0 MPa

Se-Young Chun, Heung-June Chung, Sung-Deok Hong, Sun-Kyu Yang and Moon-Ki Chung

Korea Atomic Energy Research Institute
150 Dukjin-dong Yusong-gu, Taejon 305-353, Korea
sychun@kaeri.re.kr

(Received June 7, 1999)

Abstract

The critical heat flux (CHF) experiments have been carried out in a wide range of pressures for an internally heated vertical annulus. The experimental conditions covered ranges of pressures from 0.57 to 15.01 MPa, mass fluxes of 0 kg/m^{2}s and from 200 to 650 kg/m^{2}s, and inlet subcoolings from 85 to 413 kJ/kg. The characteristics of the present data and the effect of pressure on CHF are discussed. Most of the CHFs were identified to dryout of the liquid film in the annular or annular-mist flow. For the mass flux of 200 kg/m^{2}s, there were the indications that the CHF occurred at the transition from annular to annular-mist flow in the pressure range of 3~10 MPa. For the mass fluxes of 550 and 650 kg/m^{2}s, the CHFs had a maximum value at a pressure of 2~3 MPa, and the pressure at the maximum CHF values had a trend moving toward the pressure at the peak value of pool boiling CHF as the mass flux decreased. The CHF data under a zero mass flux condition indicate that both the effects of pressure and inlet subcooling on the CHF were smaller, compared with those on the CHF with net water upward flow.

Key Words : critical heat flux (CHF), heated vertical annulus, low mass flux, two-phase flow pattern transition, wide pressure range

1. Introduction

In the boiling heat transfer system, it has been observed experimentally that, above a certain heat flux, liquid can no longer permanently wet the heater surface. This situation leads to an inordinate decrease in the surface heat transfer coefficient. This heat flux is commonly referred to as the critical heat flux (CHF). The CHF in nuclear reactors is one of the important thermal hydraulic parameters limiting the available power, because the inordinate rise of reactor fuel surface temperature under CHF conditions is sometimes sufficient to cause melting of the fuel materials. Most of the

CHF studies have been concentrated on high pressure and high flow rate conditions corresponding to normal operation ranges of light water reactors (LWRs). Therefore, though several prediction methods for the CHF, which are reliable to normal operating conditions of LWRs, have been developed, these prediction methods have a relatively narrow range of validity. The importance of CHF behavior under a low flow rate condition was pointed out earlier in relation to the analysis of accident situations for LWRs, which includes a flow transient due to the reactor circulation pump failure and a loss of coolant accident. Furthermore, in a future LWR that should adopt various passive safety features, the reactor core coolability under lower coolant flow such as natural circulation plays a key role in thermal hydraulic behavior during the operational transients and the accident situations. In order to achieve optimal design and to ensure a high degree of safety in future LWRs, the CHF characteristics under low flow conditions such as natural circulation phase must be clearly understood.

Many studies have been performed on CHF in circular, annulus and fuel bundle channels over the past forty years. A wide variety of data has been obtained for CHF in annuli, since the annulus can be regarded as a single rod bundle. Janssen and Kervinen[1] performed CHF experiments for the internally heated vertical annulus channel in the pressure range of 4.1~10 MPa and mass flux range of 175~8400 kg/m^{2}s. Becker et al.[2] obtained CHF data for annuli with an inside heater rod in the pressure range of 1.0~3.5 MPa and mass flux range of 50~650 kg/m^{2}s. Barnett[3] compiled CHF data for uniformly heated annuli at a pressure of 6.9 MPa and mass fluxes from 190 to 8400 kg/m^{2}s. In recent years, Mishima and Ishii[4], Rogers et al.[5], El-Genk et al.[6] and Park et al.[7] performed with more attention CHF experiments for very low flow (several ten kg/m^{2}s) in an internally heated annulus. Their studies were conducted in a test section with heating lengths below 0.6 m under near atmospheric pressure conditions. Also, Kumamaru et al.[8] investigated the CHF in an internally heated annulus having a heating length of 2.0 m under a high pressure of 3 MPa, a low flow of 105~320 kg/m^{2}s and mixed inlet conditions, that is, conditions in which a two phase mixture of water and steam enters the test section.

The CHF data presented in the above references did not cover a wide range of pressure conditions, and only a few experiments were performed in the low flow region (250~700 kg/m^{2}s). Consideration of the influence of pressure on CHF at low flow conditions has not been given carefully until now. This paper presents the results from CHF experiments carried out in an internally heated annulus at low flow with a wide range of pressure conditions, and the effect of pressure on CHF under low flow conditions is then characterized.

2. Experimental Description

2.1. Experimental Facility

The CHF experiments reported in this paper have been conducted in the Reactor Coolant System thermal hydraulics loop facility (RCS loop facility) of the Korea Atomic Energy Research Institute (KAERI). The principal operating characteristics of the RCS loop facility are

operating pressure	0.5~16 MPa
test section flow rate	0.03~3 kg/s
maximum water temperature	620 K
available heating power of test section	500 kW.

Figure 1 shows the flow diagram of the RCS loop facility. It basically consists of a main circulating pump, preheater, CHF test section,

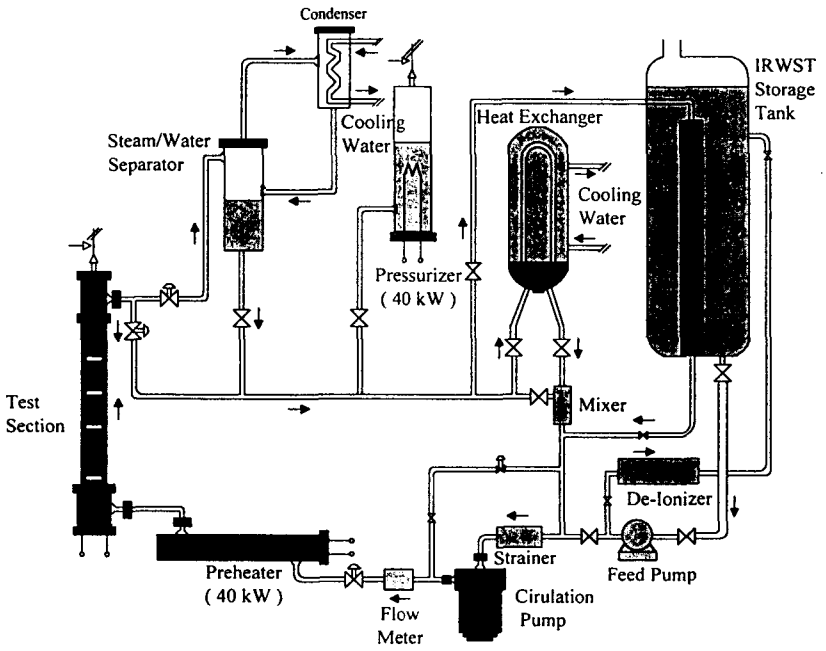

Fig. 1. Simplified Flow Diagram of the RCS Loop Facility

steam/water separator, pressurizer and cooler. Stainless steel, SUS 304, was used as construction material for the loop facility to prevent corrosion. The loop is filled with de-ionized water. The flow rate of test section inlet is controlled by the adjustments of the motor speed of the circulating pump and the flow control valve. Three kinds of orifice flow meters with different measuring ranges are installed to measure the flow rate of water entering the test section. A throttling valve located up stream of the test section inlet is used to avoid the flow fluctuations, which is usually observed under low flow conditions. The preheater with the power of 40 kW adjusts the degree of subcooling of water entering the test section. The steam generated in the test section is condensed through the condenser attached in the steam/water separator. The system pressure is maintained using the pressurizer with an immersion heater with the power of 40 kW.

Figure 2 shows the details of test section used in this experimental study. The test section which is an internally heated annulus flow channel consists of an outer pipe with a 19.4 mm inside diameter and an inner heater rod with a 9.54 mm outer diameter having a heated length of 1842 mm at room temperature. The inner heater rod is heated indirectly by electricity with uniform axial power distribution. The sheath and heating element of the heater rod are made of Inconel 600 and Nichrome, respectively. For measuring the heater rod surface temperatures and detecting CHF occurrence, six Chromel-Alumel thermocouples with a sheath outer diameter of 0.5 mm are embedded on the outer surface of the heater rod. The temperature sensing points of these thermocouples are located at 10, 30, 110, 310, 510 and 910 mm from the top end of the heated section.

The main parameters measured in this experiments are the water temperatures at the bottom and top of the heated section, the surface

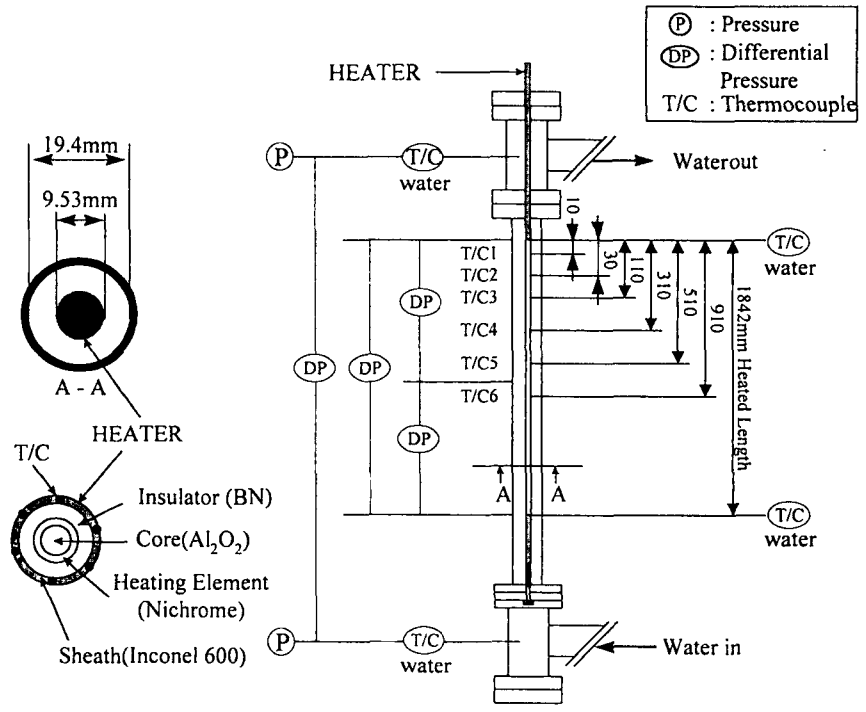

Fig. 2. Test Section Geometry and Thermocouple Locations

temperatures of the heater rod, the pressures at the inlet and outlet plenums, the differential pressures in the test section, the flow rate of the test section inlet and the power applied to the heater rod. All the electrical signals from the sensors and transmitters are treated and analyzed by a data acquisition and control system consisting of A/D and D/A converters, and a workstation computer. The uncertainties of the measuring system were estimated from the calibration of sensors and the accuracy of equipments, according to ANSI/ASME PTC 19.1 code.[9] The evaluated maximum uncertainties of pressures, flow rates and temperatures were less than ± 0.3 %, ± 1.5 % and ± 0.6 % of the readings in the range of interest, respectively. The uncertainty of the heat flux calculated from the applied power was always less than ± 1.8 % of the readings. Before starting a set of experiments, the pretests (i.e., the heat balance tests) were carried out to estimate the heat loss in the test section, so the heat loss in the test section was included in the value of heat flux.

2.2. Experimental Procedure and Conditions

CHF experiments have been performed by the following procedure. First, the flow rate, inlet subcooling and system pressure are established at desired levels, then the power is applied to the heater rod of the test section and increased gradually in small steps while the test section inlet conditions are kept at constant values. The period between the power steps are chosen sufficiently long so that the loop can be stabilized at steady state conditions. This process is continued until a sharp increase in temperature is observed in the heater rod surface. As the loop approaches CHF conditions, the temperature fluctuations of the heater rod surface are detected near the top of the

heated section. The CHF condition in the present experiments is determined when one of the surface temperatures of the heater rod continuously rises and then become 100 K higher than the saturated water temperature. Whenever the CHF is detected, the heater power is automatically reduced or tripped to prevent any damage to the heater rod.

The experiments for zero mass flux conditions are achieved by fully closing the flow control valve located down stream of the orifice flow meter, after establishing the inlet subcooling and the system pressure at desired levels.

In this work, the results of 282 CHF experiments were obtained. The experimental conditions under which the present data have been collected are as follows:

system pressure	0.57~15.01 MPa
mass flux	0 and 200~650 kg/m^{2}s
inlet subcooling	85~413 kJ/kg
exit quality	0.106~0.536

It was not always possible to keep a stable pressure in the outlet plenum near CHF conditions due to the inherent characteristics of the loop. The pressure at the inlet plenum is specified as the system pressure. The inlet subcooling is determined from the water temperature at the bottom end of the heated section and the pressure at the inlet plenum. The exit quality is thermodynamic equilibrium quality, which is calculated from the heat balance under CHF conditions. The thermodynamic properties required to analyze the data is determined from the pressure at the top end of heated section, since the CHF with net upward flow always occurred at the top end of the heated section.

In the zero mass flux experiments, the water temperature at the bottom end of the heated section was kept at a subcooled condition, even after the power was applied to the heater rod. This is due to some heat loss and convective heat transfer toward the lower plenum. Therefore, the CHF data at zero mass flux were obtained in the water subcooling from 85 to 413 kJ/kg at the bottom end of the heated section and the pressure range from 0.57 to 15.01 MPa. In the present experiments, the CHF under the zero mass flux condition always occurred at the top end of the heated section, as is the case with the CHF with net water upward flow.

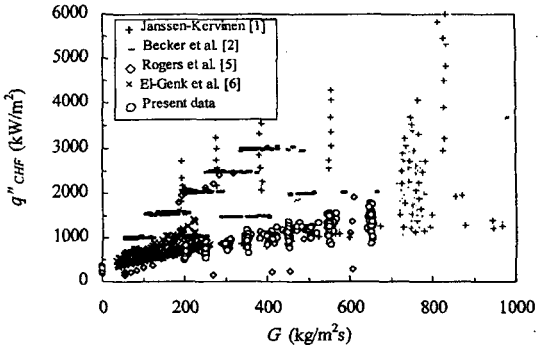

Fig. 3. CHF Data as a Function of Mass Flux

3. Experimental Results and Discussions

3.1. Characteristics of CHF

Figure 3 shows the present CHF data as a function of mass flux, together with the data of Janssen and Kervinen[1], Becker[2], Rogers et al.[5] and El-Genk et al.[6]. It is not easy to compare the present data with the existing data due to the differences in the test section geometry and inlet flow condition. However, the figure indicates that the existing data are mainly distributed in the regions below a mass flux of 250 kg/m^{2}s and beyond a mass flux of 700 kg/m^{2}s, and the data sets of Janssen and Kervinen, and Becker are comprised in a higher CHF region than the present data.

For a fixed inlet subcooling, in general, the CHF increases with increasing flow rate. Figure 4 shows

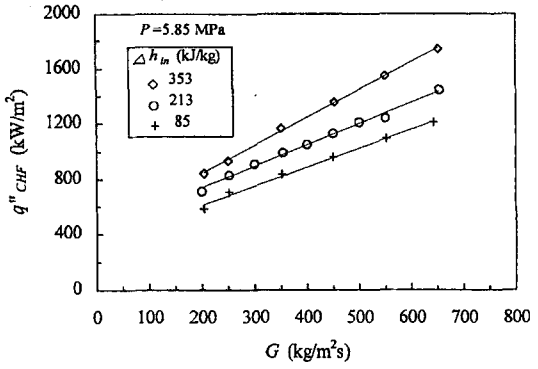

Fig. 4. CHF as a Function of Mass Flux for a Pressure of 5.85 MPa

that the CHFs rise linearly as the mass flux increases. Most of the CHF data in this experimental range indicate a trend similar to that shown in this figure. However, the departures from the linearity are observed in the data for pressures of 0.57, 1.01 and 15.01 MPa. The CHF data as a function of mass flux are shown in Figs. 5(a)~(c) with inlet subcooling as a parameter. The linear relationship between the CHF and the mass flux breaks down for the pressure of 0.57 MPa. For pressures of 1.01 and 15.01 MPa, the linearity is kept for high inlet subcooling, but is no longer kept at an inlet subcooling of 85 kJ/kg.

The CHF characteristics are closely related with the two-phase flow pattern. It is apparent that the developments of the correlation and mechanistic models for CHF require a good prediction of the flow pattern. In general, it is known that the CHF mechanisms are classified into DNB and dryout type CHF (i.e., departure from nucleate boiling and dryout of liquid film in annular flow). On the other hand, the CHF phenomenon at low flow rates is complicated because the effect of buoyancy becomes remarkable. The CHF mechanisms in a very low flow region where the mass flux is between several ten kg/m²s and several hundred kg/m²s, from the available literature (Mishima and Ishii[4], Rogers et al.[5], El-Genk et al.[6], Park et al.[7] and Kumamaru et al.[8]), are roughly classified as follows:

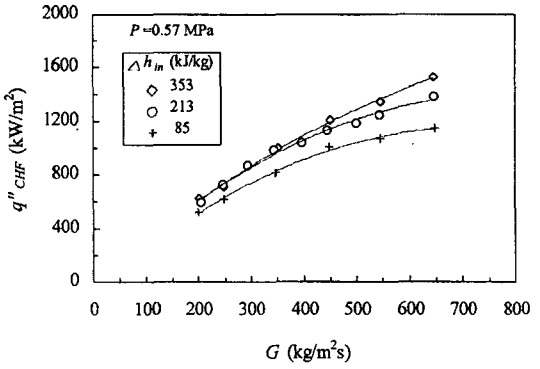

(a). 0.57 MPa

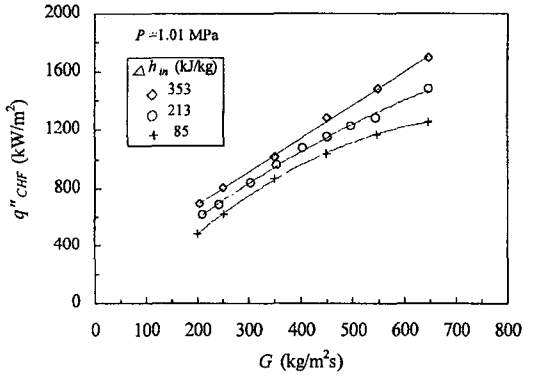

(b) 1.01 MPa

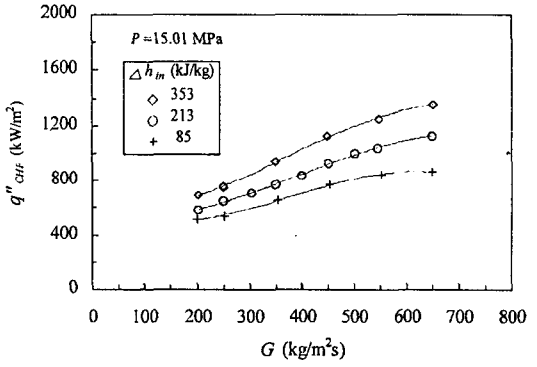

(c) 15.01 MPa

Fig. 5. CHF Data as a Function of Mass Flux

The CHF can be caused by

(a) flooding at stagnant or extremely low flow conditions,

(b) flow pattern transition from slug or churn turbulent flow to annular flow, and annular to annular-mist flow,

(c) dryout or breakup of liquid film in annular flow and

(d) complete evaporation of liquid, that is, the exit quality is about 100 % at the top of the test section, in this case, the liquid entrainment is not much.

To provide some understanding of CHF under low flow and low pressure conditions, Mishima and Nishihara[9] used two fundamental dimensionless parameters for the heat flux and the water mass flux, defined as

$$q^*_{CHF} = q''_{CHF} / [h_{fg}\sqrt{\lambda\rho_g g(\rho_f - \rho_g)}]$$

$$G^* = G/\sqrt{\lambda\rho_g g(\rho_f - \rho_g)},$$

where q^*_{CHF} is the critical heat flux, h_{fg} the latent heat of evaporation, g the gravitational acceleration, G the mass flux, ρ_f and ρ_g the densities of liquid and vapor, respectively. The length scale λ of the Taylor instability is given by

$$\lambda = \sqrt{\sigma/[g(\rho_f - \rho_g)]},$$

where σ is the surface tension. The present CHF data, including the zero flow CHFs, are plotted in terms of the dimensionless q^*_{CHF} and mass flux G^* in Fig. 6. Mishima and Nishihara indicated that churn to annular flow transition boundary given by the following equation correlates with their CHF data in the internally heated annulus:

$$q^*_{C-A} = q^*_{CF} + \frac{A_f}{A_h}\frac{\Delta h_{in}}{h_{fg}} G^*, \qquad (1)$$

where A_f is the flow area, A_h the heated area and Δh_{in} the inlet enthalpy subcooling. The dimensionless flooding CHF q^*_{CF} is expressed as follows:

$$q^*_{CF} = \frac{A_f}{A_h}\frac{C^2\sqrt{D^*}}{[1+(\rho_g/\rho_f)^{1/4}]^2}. \qquad (2)$$

In the above equation, the value of constant C describing the geometry of the test section is 0.8 for the annulus channel, and the dimensionless diameter D^* is expressed by the heated equivalent diameter D_{he} and λ as follows:

$$D^* = D_{he} / \lambda$$

El-Genk et al. [6] indicated that the CHF occurs at the transition from annular to annular-mist flow, from the visual observations and the two-phase flow pattern analyses for the flow field in their CHF experiments, and then developed the following CHF correlation for the annular to annular-mist transition:

$$q^*_{A-AM} = \frac{A_f}{A_h}\left(BN_{\mu f}^{-0.2} + E\frac{\Delta h_{in}}{h_{fg}}G^*\right), \qquad (3)$$

where B and E are the coefficients determined from the CHF data; B =0.85 and E=1.045, an d $N_{\mu f}$ is the viscosity number, defined as

$$N_{\mu f} = \frac{\mu_f}{\left\{\rho_f\sigma\sqrt{\sigma/[g(\rho_f - \rho_g)]}\right\}^{1/2}},$$

where μ_f is the viscosity of liquid. The present CHF data are compared with the churn to annular transition boundary of Mishima and Nishihara and the CHF correlation of El-Genk et al. for annular to annular-mist transition. Figure 6 shows that all the CHF data lie in the annular-mist flow region and the CHF values with low mass flux corresponding to 200 kg/m^{2}s in the medium pressures of 4.05 MPa and 5.85 MPa come close to the annular to annular-mist transition lines.

At zero flow condition with a closed bottom end

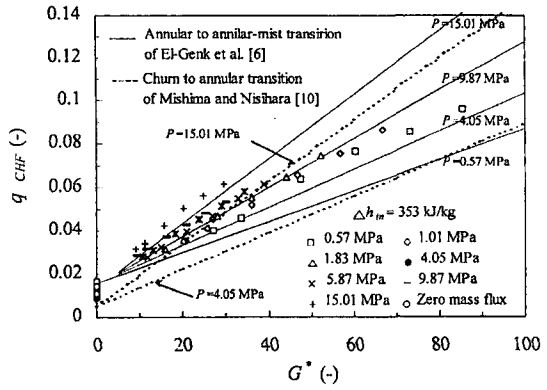

Fig. 6. Dimensionless CHF as a Function of Dimensionless Mass Flux

of the test section, a countercurrent flow is observed [6, 7, 11], that is, the vapor flows up from the heated section and on the other hand, the liquid falls down from the upper plenum due to gravity. In this case, the basic CHF mechanism is that the flooding phenomenon is the trigger of the CHF. All the CHF data at zero mass flux conditions also are plotted in Fig. 6. In the present experiments for the zero mass flux, the period between power increase steps was chosen sufficiently long (about twenty minutes) in order to maintain the stable countercurrent flow. Katto and Hirao [11] reported that the location of the onset of CHF lies between the top and bottom end of heated tube. Hwang and Chang [12] related the two-phase mixture level to the CHF location. The present experiments show that the CHFs occur at the top end of the heated section. It can be inferred that this discrepancy originates from the effects of the cold wall in the annulus channel and the unheated section above the heated section of the heater rod (see Fig. 2). The flooding CHF correlation (Eq. (2)) is based on the well-known empirical flooding correlation of Wallis [13] and the energy balance consideration. The value of constant C in the correlation (Eq. (2)) varies between 0.725 and 1.0 for tubes, depending upon the entrance shape of the test section and the fluid viscosity. If this correlation is valid for the prediction of the flooding CHF, the values of constant C in the present data have the range from 1.04 to 1.31 due to the pressure effect (i.e., the variations of vapor/liquid density ratio and viscosity).

3.2. Two-phase Flow Patterns Just Before CHF Occurrence

The churn to annular flow transition correlation (Eq. (1)) and the CHF correlation (Eq. (3)) for the annular to annular-mist transition are obtained based on the CHF experiments under near atmospheric pressure conditions and the mass fluxes lower than 260 kg/m^{2}s. Therefore, the two-phase flow pattern under CHF conditions in the present experiments are examined using the flow regime transition criteria of Mishima and Ishii [14], which can be applied over wide ranges of parameters as well as to high pressure steam-water flow. Their flow regime transition criteria are given by the following equations:

$$j_g \geq \sqrt{\frac{(\rho_f - \rho_g) g D_{hy}}{\rho_g}} (\alpha - 0.11) \tag{4}$$

for churn to annular flow transition,

$$j_g \geq \left(\frac{\sigma g (\rho_f - \rho_g)}{\rho_g^2} \right)^{1/4} N_{\mu f}^{-0.2} \tag{5}$$

for onset of droplet entrainment,

where j_g is the superficial velocity of vapor, D_{hy} the hydraulic equivalent diameter and the void fraction α is given by the following equation including the distribution parameter C_0:

$$\alpha = \frac{j_g}{C_o j + 0.35\sqrt{(\rho_f - \rho_g) g D_{hy} / \rho_f}},$$

$$C_o = 1.2 - 0.2\sqrt{\rho_g / \rho_f},$$

and

$$j = j_f + j_g,$$

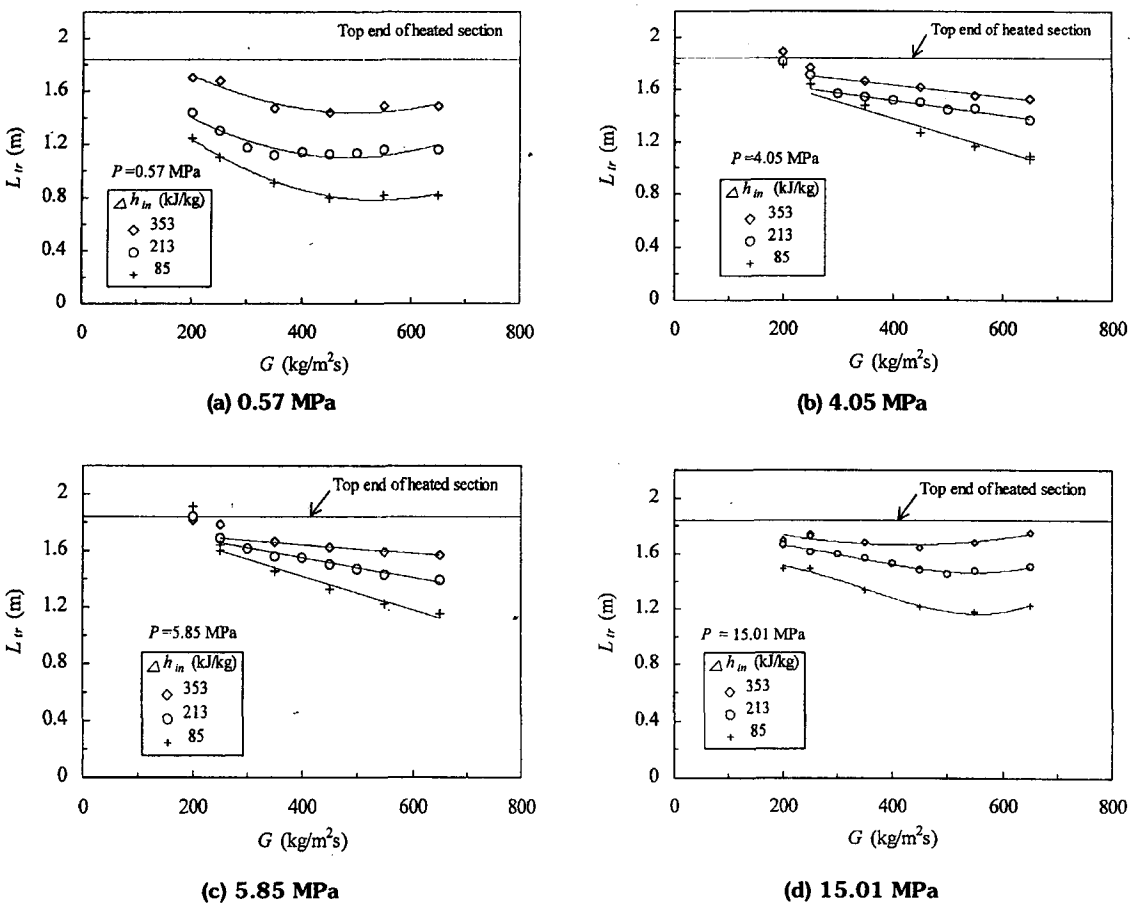

Fig. 7. Location of the Annular to Annular-mist Transition as a Function of Mass Flux at CHF Condition

where j_f is the superficial velocity of liquid. The equation (5) for the onset of droplet entrainment is applicable to predict the occurrence of the annular-mist flow. The locations of the flow pattern transitions along the heated section can be calculated from a relationship between the superficial velocity j_g (or j_f) and the equilibrium quality at flow pattern transitions x_{tr}. The location L_{tr} of transition is calculated by the following equations:

$$x_{tr} = \rho_g j_g / G,$$

and

$$L_{tr} = \frac{A_f G\left(x_{tr} h_{fg} + \Delta h_{in}\right)}{\pi d q''_{CHF}}.$$

Figure 7 shows the annular to annular-mist transition locations along the heated section under CHF conditions. The annular-mist transition locations at pressures of 4.05 and 5.85 MPa move linearly toward the lower part of the heated section with increasing mass flux, excluding the data points for the mass flux of 200 kg/m^{2}s (Fig. 7(b) and (c)). On the other hand, Figs. 7(a) and (d) for the pressures of 0.57 and 15.01 MPa show

that the annular-mist transitions do not move simply downward along the heated section in proportion to the mass flux. These features on the annular-mist transition originate from the fact that the linear relationship between the CHF and the mass flux breaks down under low and high pressure conditions, as shown Fig. 5. The annular to annular-mist transitions for the mass flux of 200 kg/m^{2}s in the pressures of 4.05 and 5.85 MPa occur very close to the top end of the heated section (i.e., the location of CHF occurrence). The locations of annular-mist transitions are discontinuous with those for the mass fluxes of not less than 250 kg/m^{2}s and jump to the top end line of the heated section. In the present conditions, Figs. 6 and 7 demonstrate that the CHF mechanism is almost identified to dryout of the liquid film in the annular flow or annular-mist flow, excluding a few CHF data at the mass flux of 200 kg/m^{2}s in the medium pressures.

3.3. Effect of Pressure

The locations of the two-phase flow transitions under CHF conditions are plotted as a function of the pressure in Fig. 8. The superficial vapor velocity in equation (5) for the annular to annular-mist transition depends only on the fluid properties, but equation (4) for the churn to annular transition includes the geometric parameters such as hydraulic diameter and void fraction. In the annuli, the two-phase flow situations may be different from those of the tubes, because of the existence of the effects of the annular gap and cold wall. However, the application of equation (4) to the present data is useful to understand the general two-phase flow behaviors under CHF conditions. Figure 8(a) shows that at medium pressures from 3 to 10 MPa, the locations of the flow pattern transitions for the mass flux of 650 kg/m^{2}s move simply

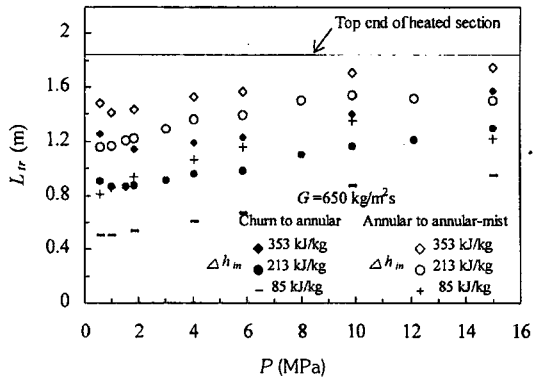

(a) 650 kg/m^{2}s

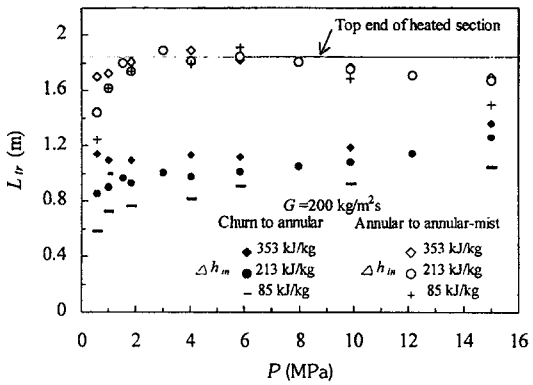

(b) 200 kg/m^{2}s

Fig. 8. Effect of Pressure on the Location of Flow Pattern Transition at CHF Condition

down stream of the heated section as the pressure is increased. On the contrary, as shown in Fig. 8(b) for the mass flux of 200 kg/m^{2}s, at medium pressures, the flow pattern transitions take place at approximately constant locations independent of pressure. The locations of annular to annular-mist transition at the mass flux of 650 kg/m^{2}s are greatly influenced by the subcooling of the test section inlet. However, in the case of the mass flux of 200 kg/m^{2}s, the effect of the inlet

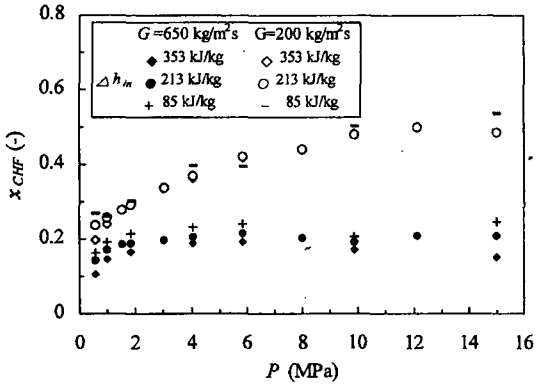

Fig. 9. Effect of Pressure on CHF at an Inlet Subcooling of 213 kJ/kg

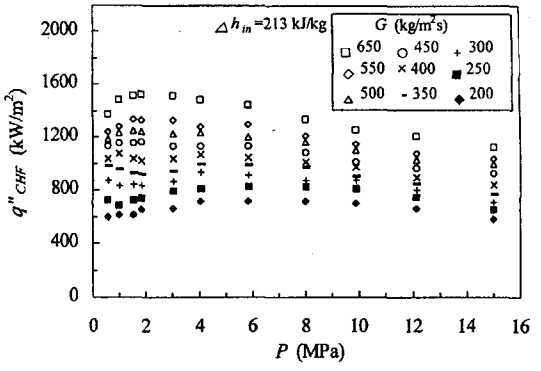

Fig. 10. Effect of Pressure on CHF at an Inlet Subcooling of 213 kJ/kg

subcooling on the locations of annular to annular-mist transition is very small. As shown in Fig. 7, it was pointed out that the transitions to annular-mist flow for the mass flux of 200 kg/m^{2}s at the pressures of 4.05 and 5.85 MPa occur very close to the location where the CHF takes place. Figure 8 (b) also indicates that annular flow changes into annular-mist flow near the top end of the heated section in the pressure range from 3 to 10 MPa at the mass flux of 200 kg/m^{2}s. This transition characteristic supports the experimental results of El-Genk et al. [6], that the CHF occurred at the transition from annular to annular-mist flow.

The exit quality under CHF conditions (i.e., the critical quality x_{CHF}) is shown as a function of the pressure in Fig. 9. The critical qualities for the mass flux of 200 kg/m^{2}s increase as the pressure increases and are always greater than those for the mass flux of 650 kg/m^{2}s, throughout a range of pressures. However, unlike the low mass flux conditions, in the high mass flux (650 kg/m^{2}s), the values of the critical qualities vary scarcely at pressures above 3 MPa. The critical qualities for the inlet subcooling of 353 kJ/kg rather have a trend to decrease in the high pressure region (above 10 MPa). Figures 8 and 9 implies that the droplet entrainments are easy to be caused from the liquid film in the high mass flux because the vapor velocity is high enough.

In order to illustrate the effect of pressure on CHF, the present data are plotted in Fig. 10 as a function of pressure. For the mass fluxes of 550 and 650 kg/m^{2}s, the CHFs have a common feature that the CHF increases rapidly as the pressure increases and then a maximum value of CHF appers at a pressure of 2~3 MPa, and above this pressure, CHF decreases slowly with a further increasing pressure. For the mass flux of 300~500 kg/m^{2}s in lower inlet subcooling, the rapid increase of the CHF is not observed in the low pressure region. In the low mass fluxes (200 and 250 kg/m^{2}s), the effect of pressure is not so remarkable. Also, the CHF data as a function of the pressure are shown in Fig. 11 with the inlet subcooling as a parameter. In regard to the effect of pressure on CHF, there are the available data of Bowditch and Mogford [15], who performed CHF experiments for 5×5 heater rods bundle geometry in a pressure range of 2~16 MPa. Their CHF data indicated that the CHF had a peak value at a pressure of about 4 MPa, and the effect of pressure on the CHF is not observed under low mass flux (below 300 kg/m^{2}s) and low inlet subcooling (50 kJ/kg) conditions. In the case

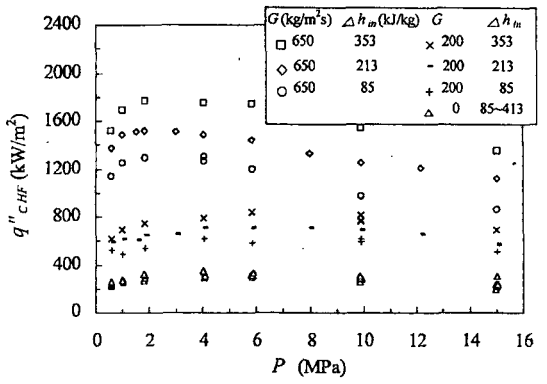

Fig. 11. Effect of Pressure on CHF at Fixed Mass Flux Conditions

of pool boiling (Morozov [16]), it is known that CHF reaches a maximum at one third of the critical pressure (about 8 MPa). From Figs. 10 and 11, it is found that the CHF in the high mass flux have a maximum value at pressure of 2~3 MPa, and the pressure at the maximum CHF values has a trend moving toward the pressure at the peak value of pool boiling CHF as the mass flux is decreased. As shown in Fig. 11, both the effects of pressure and inlet subcooling on the CHF for the zero mass flux are smaller, compared with those on the other CHF. As mentioned above, the CHF under zero mass flux conditions with a closed bottom end of the test section is different from the pool boiling CHF, and the flooding phenomenon causes the CHF. Consequently, the CHF values at zero mass flux do not have a clear peak value for the variation of the pressure.

4. Conclusions

The CHF experiments have been carried out in an internally heated vertical annulus. The experimental conditions covered ranges of pressures from 0.57 to 15.01 MPa, mass fluxes of 0 kg/m^{2}s and from 200 to 650 kg/m^{2}s and inlet subcoolings from 85 to 413 kJ/kg. The CHF data for the region where the existing CHF data are insufficient were collected. The following conclusions can be drawn from this study;

(1) Most of the CHF data in the present experimental ranges rise linearly as the mass flux increases. The departures from the linear relationship between the CHF and the mass flux are observed in the data for pressures of 0.57, 1.01 and 15.01 MPa.

(2) In the present conditions, most of the CHFs are identified to dryout of the liquid film in the annular or annular-mist flow. For the mass flux of 200 kg/m^{2}s, the considerations of the two-phase flow pattern give the indications that the CHF may occur at the transition from annular to annular-mist flow in the pressure range 3~10 MPa.

(3) For the mass fluxes of 550 and 650 kg/m^{2}s, the CHFs increase rapidly as the pressure increases and then have a maximum value at a pressure of 2~3 MPa. Above this pressure, the CHFs decrease slowly with further increasing pressure. The pressure at the maximum CHF values has a trend moving toward the pressure at the peak value of pool boiling CHF as the mass flux is decreased.

(4) The CHF under zero mass flux conditions is caused by the flooding phenomenon in a countercurrent flow, and both the effects of pressure and inlet subcooling on the CHF are smaller, compared with those on the CHF with net water upward flow. Therefore, the CHF values at zero mass flux do not have a clear peak value for the variation of the pressure.

Nomenclature

A_f cross sectional flow area [m^2]
A_h heated area [m^2]
B coefficient in equation (3) [-]
C constant in the Wallis correlation for

flooding [-]

C_0 distribution parameter [-]

D^* dimensionless diameter [-]

D_{he} heated equivalent diameter [m]

D_{hy} hydraulic equivalent diameter [m]

d outer diameter of heater rod [m]

E coefficient in equation (3) [-]

G mass flux (kg/m^{2}s)

G^* dimensionless mass flux [-]

g gravitational acceleration [m/s^2]

h_{fg} latent heat of evaporation [kJ/kg]

Δh_{in} inlet subcooling enthalpy [kJ/kg]

j superficial velocity of two-phase mixture [m/s]

j_f superficial liquid velocity [m/s]

j_g superficial vapor velocity [m/s]

L_{tr} location of two-phase flow pattern transition [m]

$N_{\mu f}$ dimensionless viscosity number [-]

P pressure [MPa]

q''_{CHF} critical heat flux [kW/m^2]

$q^*_{A\text{-}AM}$ dimensionless heat flux at annular to annular-mist transition [-]

$q^*_{C\text{-}A}$ dimensionless heat flux at churn to annular transition [-]

q^*_{CF} dimensionless critical heat flux due to flooding [-]

q^*_{CHF} dimensionless critical heat flux [-]

x_{CHF} quality at critical heat flux condition [-]

x_{tr} quality of location at two-phase flow pattern transition [-]

Greek symbols

α void fraction [-]

λ length scale of the Taylor wave [m]

μ_f dynamic viscosity of liquid [Ns/m^2]

ρ_f density of liquid [kg/m^3]

ρ_g density of vapor [kg/m^3]

σ surface tension [N/m]

Acknowledgment

This work was supported by the financial support for the nuclear R & D program from the Ministry of Science and Technology of Korea.

References

1. E. Janssen and J. A. Kervinen, "Burnout conditions for single rod in annular geometry, water at 600 to 1400 psia," General Electric Company, Atomic Energy Commission, USA, GEAP-3899 (1963).
2. K. M. Becker et al., "Burnout data for flow of boiling water in vertical round duct, annuli, and rod clusters," Aktiebolaget Atomenergi, Stockholm, Sweden, AE-177 (1965).
3. P. G. Barnett, "A correlation of burnout data for uniformly heated annuli and its use for predicting burnout in uniformly heated rod bundles," AEEW-R463 (1966).
4. K. Mishima and M. Ishii, "Experimental study on natural convection boiling burnout in annulus," Proceeding of the 7th International Heat Transfer Conference, Munchen, 4, 309-314 (1982).
5. J. T. Rogers et al., "Flow boiling critical heat fluxes for water in a vertical annulus at low pressure and velocities," Proceeding of the 7th International Heat Transfer Conference, Munchen, 4, 339-344 (1982).
6. M. S. El-Genk et al., "Experimental studies of critical heat flux for low flow of water in vertical annuli at near atmospheric pressure," Int. J. Heat Mass Transfer, 31, 2291-2304 (1988).
7. J.W. Park et al., "Critical heat flux and flow pattern for water flow in annular geometry," Nucl. Eng. Des., 172, 137-155 (1994).
8. H. Kumamaru et al., "Critical heat flux for annulus under high-pressure, low-flow and mixed inlet conditions," J. Nucl. Sci. Tech.,

27[1], 68-80 (1990).

9. ANSI/ASME PTC 19.1, "ASME Performance test codes, supplement on istruments and apparatus, part 1, measurement uncertainty," (1985).
10. M. Mishima and H. Nishihara, "Effect of channel geometry on critical heat flux for low pressure water," Int. J. Heat Mass Transfer, 30, 1169-1182 (1987).
11. Y. Katto and T. Hirao, "Critical heat flux of counter-flow boiling in a uniformly heated vertical tube with a closed bottom," Int. J. Heat Mass Transfer, 34, 993-1001 (1991).
12. D. H. Hwang and S. H. Chang, "Development of a phenomenological model for the prediction of dryout locations under flooding-limited critical heat flux conditions," Nucl. Eng. Des., 148, 475-486 (1994).
13. G. B. Wallis, "One-dimensional two-phase flow," McGraw-Hill Book Company, 336-342 (1969).
14. K. Mishima and M. Ishii, "Flow regime transition criteria for upward two-phase flow in vertical tube," Int. J. Heat Mass Transfer, 27, 723-737 (1984).
15. F. H. Bowditch and D. J. Mogford, "An experimental and analytical study of fluid flow and critical heat flux in PWR fuel elements," AEE Winfrith, AEEW-R2050 (1987).
16. V. G. Morozov, "New experimental data on critical heat loads at boiling of liquids on a submerged heating surface," Int. J. Heat Mass Transfer, 5, 661-666 (1962).